BEAM-INDUCED HEAT LOAD PREDICTIONS AND MEASUREMENTS IN THE APS SUPERCONDUCTING UNDULATOR*

Katherine C. Harkay[#], Laura Boon, Michael Borland, Yong-chul Chae, Roger Dejus,
Jeffrey Dooling, Charles Doose, Louis Emery, Yury Ivanyushenkov, Mark Jaski,
Matthew Kasa, Suk H. Kim, Robert L. Kustom, Vadim Sajaev, Yuko Shiroyanagi, Xiang Sun
ANL, Argonne, IL 60439, USA

Abstract

The first test superconducting undulator (SCU0) was successfully installed and commissioned at the Advanced Photon Source (APS) and is delivering 80- to 100-keV photons for user science. The cryosystem was designed to handle a beam-induced heat load of 40 W. Prior to operations, detailed predictions of this heat load were made, including that produced by resistive wall heating by the image current, geometric wakefields, synchrotron radiation, electron cloud, and beam losses. The dominant continuous wave (cw) source is the resistive wall heat load. The heat load predictions for standard 100-mA user operation were benchmarked using thermal sensors that measure temperatures along the SCU0 beam chamber. Analysis using the predicted heat loads from the electron beam agrees well with the observed measurements.

INTRODUCTION

A test superconducting undulator (SCU0) has been developed at APS [1] and was recently installed in the storage ring. A key design criterion was a vacuum and cooling system that keeps the NbTi coils cooled to 4 K in the presence of heating caused by the electron beam passing through the undulator beam chamber. The SCU0 beam chamber cooling system was designed for 40 W (at 20 K) of cooling capacity based on preliminary calculations of the beam-induced heat load [2]. In this paper, updated predicted heat loads are compared with measurements carried out during SCU0 commissioning [3].

Sources of beam-induced heat load on the SCU0 beam chamber include resistive-wall heating due to beam-induced image currents, synchrotron radiation generated in upstream dipole magnets, wakefield effects, direct beam interception and, potentially, electron cloud-induced multipacting effects. Under nominal operating conditions cw heat loads are present, while specific machine fault conditions may occur that give rise to individual transient heat loads.

Estimates of the various contributions to the heat load due to the beam are shown in Tables 1 and 2 for cw and transient sources, respectively, assuming 24-bunch operation. The central part of the chamber is nominally 20 K and is thermally isolated from the 4-K magnetic structure. The chamber transitions are in the 60- to 300-K cold-to-warm transition region. Where appropriate, the heat loads at 20 K and 60/300 K are given separately.

Table 1: Estimated cw Beam-induced Heat Loads on the SCU0 Chamber, in 100-mA User Operations

Heat Source	Value at 20 K (60/300 K)
Resistive wall	4.7 W (11.3 W)
Wakefields	< 0.5 W (0.8 W)
Injection losses	2 W (non-top-up mode)
	0.1 W (top-up mode)
Synchrotron radiation	0.2 W
Beam lifetime losses	<< 1 W
Electron cloud	< 2 W
Total heat load	10 W (12 W)

Table 2: Estimated Max. Transient Beam-induced Heat Loads on the SCU0 Chamber, in 100-mA User Operations

Heat Source	Value
Injected beam loss	13 W
Corrector failure	20 W
Synchrotron radiation with steering errors	25 W
Electron beam steering errors	20 W
Max. transient heat load	25 W

MEASUREMENTS

The beam-induced heating on the SCU0 beam chamber was measured using nine Cernox cryogenic thermal sensors mounted on the beam chamber, shown in Fig. 1 (Temp0-8). Sensors Temp2-6 are mounted on the outboard side of the aluminum section of the chamber, and Temp0,1,7,8 are mounted on the top side of the stainless steel (SS) cold-to-warm transition. The chamber heater is connected to a copper block mounted adjacent to sensor Temp5. A calibrated heat load was applied to the heater using a variable power supply. The chamber heater was used to calibrate the thermal sensors, allowing determination of the heat load from the temperature measurements. This calibration was used to both predict and benchmark the chamber temperatures for storage ring beam operation.

Chamber Heater Calibration

To simulate SCU0 operating conditions, the main coil current was set to 500 A, but there was no stored beam. An external supply current was used to vary the chamber heater power based on the known heater resistance. The chamber temperatures were recorded for P=0, 5, 10, 20, and 30 W, waiting 10-20 min per step. The equilibrium chamber temperatures were determined by fitting the measurements to an exponential function. The zero-power
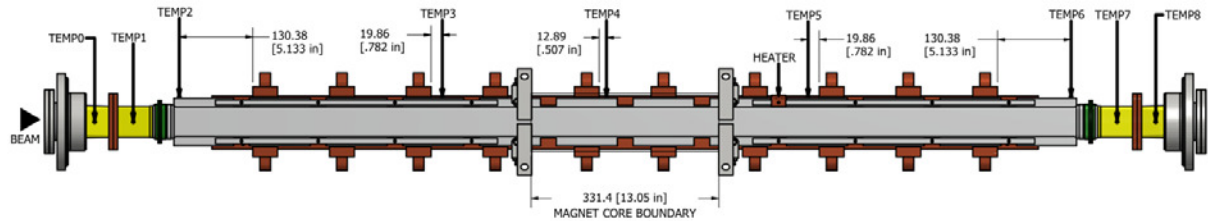
Figure 1: Thermal sensor (TEMP 0-8) locations are noted on a SCU0 beam chamber schematic, top view. The chamber heater is adjacent to TEMP5. Copper thermal links, shown in brown, connect the chamber to the cryocoolers via a common Cu bar. The Al section of the chamber is shown in grey and the stainless steel (SS) section in yellow.

temperature was averaged over 15 min prior to the start of the heater studies.

The temperature gains vs. chamber heater power for sensors 1-7 are shown in Fig. 2 as a function of their positions, s. Sensor 5 shows the largest temperature gain, as expected. The adjacent sensors 4 and 6 show a much smaller temperature gain; heat is extracted between these points by thermal links to the cryocoolers. Ideally, the heater on the Cu bar connecting all the thermal links could have been used, but the heat transfer is not known between the Cu bar and the chamber. The chamber heater calibration is also not exact, but was implemented knowing these limitations.

Because the chamber heater and sensor 5 are collocated between the same thermal links, sensor 5 is used to calibrate the temperature response to a known heat load. A polynomial fit for the temperature gain ΔT as a function of calibrated power P gives:

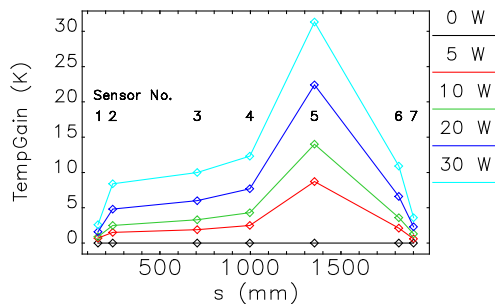$$\Delta T = 1.974P - 0.0667P^2 + 0.00119P^3 \qquad (1)$$

Figure 2: Chamber heater results for sensors 1-7, shown as a function of their positions, s.

Results

The chamber temperatures under stable cw conditions (no beam injection) were predicted using the dominant resistive-wall heat load only. In Table 1, the heat load at 20 K was obtained by multiplying the linear power density over the entire Al chamber length of 1.62 m. The power density varies with the number of bunches; for 24 bunches, it is 2.88 W/m [4,5]. However, the heater calibration should only be valid in the segments within the thermal links, a total length of 1.33 m. Therefore, this shorter length was used to estimate P, and the expected temperature gain was computed using Eq. (1). Also, the

calibration was only applied to the central sensors 3-5, since these three sensors are located between thermal links. The baseline, no-beam temperature of the Al chamber central region is 7 K. The predicted power and expected final temperatures ($7\,K + \Delta T$) are given in Table 3 for the three standard bunch patterns at 100 mA (nominal user operations), and for 324 bunches at 150 mA (special operations). These predictions were available prior to SCU0 commissioning. The measured temperature (averaged at sensors 3-5) is also shown in the table, and the agreement with the expectations is very good. Finally, the power inferred from the measured temperatures was determined using Eq. (1) and is listed in the table.

Table 3: Comparison of Predicted and Measured SCU0 Chamber Heat Load and Temperatures at Sensors 3-5.

Beam current (mA)	No. bunches	Predicted power (W)	Expected T (K)	Msrd T (K)	Inferred power (W)
100	24	3.8	13.6	12.8	3.3
100	1+56	2.7	11.8	11.9	2.7
100	324	0.5	7.9	8.2	0.6
150	324	1.2	9.3	9.5	1.3

DISCUSSION

The SCU0 cryogenic system performed very well in the presence of the beam, with the magnet temperatures being maintained near 4 K while the beam chamber center temperature reached ~13 K. The 20-K cooling system for the beam chamber, with its 40-W capacity, provides a comfortable margin for normal user operation.

The predicted cw heat load, using only the resistive-wall heating, agrees remarkably well with the measurements using the chamber heater calibration. An independent thermal modeling using finite-element analysis also gives very good agreement with the measured temperatures over the entire length of the chamber [6]. The resistive-wall heating calculation for the Al section includes the anomalous skin effect, where the skin depth is small compared to the electron mean-free path. In this regime, only a fraction of the conduction electrons carry the current, which effectively decreases the wall conductivity [7]. The anomalous skin effect begins to show a difference for a resistivity ratio (RR) > 9 [5]; at 20 K, RR = 11 for 6063-T5 Al. The surface

resistance also increases with surface roughness, and the effect can be computed using an empirical formula. For the SCU0 chamber, a surface roughness of 0.2 μm rms would increase the power loss by as much as 15% [4]. The SCU0 Al chamber was processed using an abrasive-flow polishing technique [8], and the measured surface roughness is on the order of 0.1 μm rms [9]; therefore, the surface roughness effect could be neglected.

All other contributions to the heat load are inferred to be small. The predicted synchrotron radiation heat load of 0.2 W in Table 1 [10-12] is small compared to the resistive-wall heat load for all bunch patterns except for the 324-bunch mode, where the predicted temperatures are underestimated. If the electron beam was mis-steered in the upstream dipole or corrector magnets and/or the chamber was not well-aligned, the synchrotron radiation heat load could be much higher, up to 25 W [13]. The results suggest that both the beam steering and the chamber alignment are within tolerance. The surface roughness of the SCU0 beam chamber has another effect: it can increase the synchrotron radiation absorption in the SCU0 chamber, which can increase the heat load. While this effect has not yet been analyzed, the results in Table 3 suggest that if it exists, the effect is very small.

Wakefields are predominantly in the chamber transitions outside the SCU0 cryostat, and the heat load was predicted to be dissipated primarily in the cooled Cu tapered transition upstream of the SCU0 [14]. The results in Table 3 are consistent with the absence of significant wakefield heating in the center of the chamber. Any potential heat load from beam lifetime losses is also inferred to be negligible, as predicted in Table 1.

So far, there is no evidence of anomalous heat loads on the SCU0 chamber. This is noteworthy, since measured beam-induced heat loads that are 2-10 times greater than what was expected have been reported for in-vacuum superconducting wigglers [15] and in-vacuum cryocooled permanent magnet undulators [16]. In the case of MAX [15], the discrepancy is assumed to depend on the fact that the Cu plating of the inner surfaces of the cold bore has a lower electrical conductivity than foreseen. The SCU0 is an out-of-vacuum device designed with a solid Al chamber wall for which resistive-wall heating is well understood. Calculations predict that high-current closely spaced bunches (such as in the case of 324 bunches) are more likely to drive an electron-cloud-induced multipacting resonance in the APS [2]. In SCU0 so far, there is no evidence of multipacting. Multipacting is believed to be responsible for an anomalous beam heat load and pressure rise at the ANKA in-vacuum superconducting undulator [17].

TRANSIENT HEAT LOADS

Transient heat load predictions in Table 2 assumed that the power is incident on the beam chamber. The maximum transient heat load of 25 W is within the SCU0 cooling capacity. The device was found to quench during unintentional beam dumps that have occurred during user operation due to fault conditions unrelated to SCU0. A beam loss in the magnet coils of ~1 nC (< 0.3% of the full store) could potentially cause a quench [18]. Procedures to mitigate these quenches are under investigation. With the exception of beam dumps, the device has quenched only twice in eight months of user operations, operating above its 500-A design current. The SCU0 magnet current is switched off prior to intentional beam dumps and during machine studies to avoid quenching.

SUMMARY

The cw beam-induced heat load predictions for the SCU0 beam chamber in standard APS user operation were compared with measurements using a simple chamber heater calibration. The expected chamber temperatures were used as a guide during SCU0 commissioning. The agreement between the expected and measured temperatures was very good, within 10%. The resistive-wall heat load is the dominant source, and all other contributions are inferred to be small, as predicted. There were no anomalous heat load sources detected. The SCU0 cryogenic system performed very well in the presence of the beam, as designed.

ACKNOWLEDGMENT

REFERENCES

[1] Y. Ivanyushenkov et al., IEEE Trans. on Applied Superconductivity, 21 (2011) 1717; Y. Ivanyushenkov et al., Proc. IPAC2012, MOPPP078, p. 744 (2012); journals.iucr.org/s/issues/2013/03/00/s130300aps.pdf

[2] M. Petra, R.L. Kustom, private communication (2004); R.L. Kustom, private communication (2010).

[3] K. Harkay et al., WEOAA3, NA-PAC'13.

[4] R.L. Kustom, private communication (2011, 2012).

[5] S.H. Kim, APS Light Source Note ANL/APS/LS-329 (2012).

[6] Y. Shiroyanagi et al., THPAC07, NA-PAC'13.

[7] B. Podobedov, PRST-AB 12 (2009) 044401.

[8] E. Trakhtenberg et al., Proc. PAC2011, p. 2093 (2011).

[9] L. Boon, K. Harkay, Proc. 2012 Electron Cloud Workshop (ECLOUD12), Isola d'Elba, Italy (2012).

[10] M. Jaski, private communication (2012).

[11] R. Dejus, private communication (2012).

[12] L. Boon et al., Proc. IPAC2011, THPC186, p. 3332 (2011).

[13] L. Boon et al., THPAC06, NA-PAC'13.

[14] L. Emery, X. Sun, private communication (2013).

[15] E. Wallen and G. LeBlanc, Cryogenics 44 (2004) 879.

[16] P. Elleaume, "Cryogenic Permanent Magnet Undulator Development at the ESRF," Three-Way Meeting, Argonne; http://www.aps.anl.gov/News/Conferences/2008/3WM08/3WM08Accelerator_R&D.htm

[17] S. Casalbuoni et al., PRST-AB 13 (2010) 073201.

[18] J. Dooling, private communication (2013).